Available online at www.sciencedirect.com

SciVerse ScienceDirect

journal homepage: www.elsevier.com/locate/jmbbm

Research paper

A constrained mixture approach to mechano-sensing and force generation in contractile cells

*Franck J. Vernerey**, *Mehdi Farsad*

Department of Civil, Environmental and Architectural Engineering, University of Colorado, Boulder, USA

ARTICLE INFO

Article history:
Received 9 February 2011
Received in revised form
6 May 2011
Accepted 9 May 2011
Published online 17 May 2011

Keywords:
Cell mechanics
Mixture theory
Mechano-sensing
Cell contractility

ABSTRACT

Biological tissues are very particular types of materials that have the ability to change their structure, properties and chemistry in response to external cues. Contractile cells, i.e. fibroblasts, are key players of tissue adaptivity as they are capable of reorganizing their surrounding extra-cellular matrix (ECM) by contracting and generating mechanical forces. This contractile behavior is attributed to the development of a stress-fiber (SF) network within the cell's cytoskeleton, a process that is known to be highly dependent of the nature of the mechanical environment (such as ECM stiffness or the presence of stress and strain). To describe these processes in a consistent manner, the present paper introduces a mutiphasic formulation (fluid/solid/solute mixture) that accounts for four major elements of cell contraction: cytoskeleton, cytosol, SF and actin monomers, as well as their interactions. The model represents the cross-talks between mechanics and chemistry through various means: (a) a mechano-sensitive formation and dissociation of an anisotropic SF network described by mass exchange between actin monomer and polymers, (b) a bio-mechanical model for SF contraction that captures the well-known length–tension and velocity–tension relation for muscles cells and (c) a convection/diffusion description for the transport of fluid and monomers within the cell. Numerical investigations show that the multiphasic model is able to capture the dependency of cell contraction on the stiffness of the mechanical environment and accurately describes the development of an oriented SF network observed in contracting fibroblasts.

Published by Elsevier Ltd

1. Introduction

Biological tissues are very particular types of materials that have the ability to change their structure, properties and chemistry in response to external cues. This fast response capability can be attributed to the out-of-equilibrium nature of the tissue structure, resulting from a constant cross-talk between a population of cells and their surrounding extra-cellular matrix (ECM). These interactions allow cells to sense stimuli conveyed by the ECM (Lambert et al., 1998) (such as force, deformation or flow) and the ECM to restructure due to the action of cells (characterized by traction forces Tamariz and Grinnell, 2002; Dallon and Ehrlich, 2008 or enzyme degradation Vernerey et al., in press). In this context, a large number of studies have demonstrated that cell contraction and architecture were strongly dependent on substrate stiffness (Wang et al., 2000; Solon et al., 2007; Guo et al., 2006; Levental et al., 2006), giving mechanics

* *Corresponding author.*
E-mail address: franck.vernerey@colorado.edu (F.J. Vernerey).

1751-6161/$ - see front matter. Published by Elsevier Ltd
doi:10.1016/j.jmbbm.2011.05.022

a central role in cell-substrate interactions. Experimental studies on contractile cells (such as myofibroblasts) generally show that larger substrate stiffness results in higher cell stability that manifests itself by large spreading areas and generation of significant traction forces. In addition, actin staining procedures have shown that fibroblast contraction is associated with the formation of highly aligned stress-fibers (SF) within the cell's structure (cytoskeleton) that anchor at the point of cell-substrate adhesion and often span the entire length of the cell. The distribution and orientation of these fibers correlate very well with the presence of contractile forces applied by cells to their underlying substrate. These phenomena clearly illustrate the intricate interplay between mechano-sensing, force generation and cytoskeletal structure, which is essential to tissue remodeling.

Despite our more and more accurate understanding of the molecular mechanisms responsible for contraction, there are still many questions concerning the nature and mechanisms of mechano-sensing and force generation (Vernerey, 2010). To tackle these questions, it is necessary to develop mathematical models that are capable of describing the cross-talk between cellular mechanics and biochemistry in a quantitative fashion. From a modeling standpoint, cell contractility has often been considered in terms of prestress or prestrain, either within the context of fibrous networks (Mohrdieck et al., 2005) or continuum mechanics (Nelson et al., 2005; Vernerey and Farsad, 2011). While such simplified models capture well the mechanical aspects of cell contraction, they are unable to explain many features occurring from chemo-mechanical interaction at the molecular scale, such as dependency of contractility on substrate stiffness and ligand density. More recent studies by Deshpande et al. (2006, 2008) introduced a bio-mechanical model that is able to describe cytoskeleton contraction by considering molecular mechanisms associated with SF formation and focal adhesion assembly. This approach provides a promising means of capturing the chemo-mechanics of cell contraction but it neglects the multiphasic aspect of the cell's body in which monomer transport, interstitial fluid (cytosol) pressure and mass exchange can take place. The inclusion of the above physics is critical to respect fundamental physical principles such as mass conservation, but also in capturing key cellular phenomena such as osmotic loading and transport phenomena. In continuum mechanics, these types of phenomena have traditionally been described by the theory of porous media and mixtures Biot (1941, 1957); Truesdell and Noll (1965); Bowen (1980); Rajagopal and Tao (1995); Sun et al. (1999); Vernerey et al. (in press); these formulations were very successful in describing phenomena such as growth Humphrey and Rajagopal (2002); Garikipati et al. (2004), free swelling (Sun et al., 1999) and osmosis (Gu et al., 1999). Applications to the cell have thus far been limited to the flow-dependent mechanical response and swelling behavior of chondrocytes in response to their osmotic environment (Guilak et al., 2006).

The present paper proposes to extend the range of applications of mixture models to describe the coupled biochemical/mechanical processes responsible for cell contraction. The formulation is based on a description of cells that incorporate four key components of contractility: a passive solid cytoskeleton, an interstitial fluid representing the cytosol, an anisotropic network of SF and a pool of globular actin monomers that freely diffuse in the cytosol. To address the well known difficulties regarding stress partitioning and boundary conditions associated with classical theory of mixtures (Rajagopal and Wineman, 1990), we take the following approach. First, it is assumed that the two solid constituents (passive cytoskeleton and SF) undergo the same motion, which is consistent with the class of constrained mixture models introduced in Humphrey and Rajagopal (2002). Second, we adopt key concepts of poromechanics (Terzaghi, 1943) that consist of describing the motion of a fluid's constituents relative to solid constituent through diffusion-type relation (initially originated by Fick and Darcy). In this context, the mixture problem is well-posed and provides a flexible and robust theoretical framework to study the interactions between mechanics and chemistry (incorporating mass and energy exchange between constituents). The key features of the proposed model are as follows: (a) The SF network is described in statistical terms with a Von Mises distribution whose characteristics (mean, deviation) evolve in time. (b) The generation of contractile force by SF follows length–tension and velocity–tension curves that are known to accurately capture the behavior of sarcomeric structures. (c) The anisotropic formation and dissociation of the SF network depend on the level of contractile stress in existing SF and (d) SF formation is limited by the diffusion and quantity of globular actin monomers present in the cytoplasm. By capturing these important physics, we show that the formulation is capable to reproducing the mechano-sensitivity of cell contraction with respect to substrate stiffness as well as the general architecture of contractile cells.

The paper is organized as follows. In the next section, we provide the basis for the continuum description of the cell's body that contains both kinematics and structural components. Section 3 then concentrates on the conservation and exchange of mass occurring within the cell during contraction while mechanical equilibrium, SF contractility and cell elasticity are discussed in Section 4. Results and predictions of the proposed model are then described in Section 5 in which several problems are considered together with comparisons with experimental studies. A general discussion of the model, potential improvements and concluding remarks are finally provided in Section 6.

2. Constrained mixture description of cells

2.1. *Continuum assumptions and kinematics*

From a material's view point, a cell can be considered as a complex composite structure, composed of a large variety of interacting constituents, which may be solid (such as microtubules, actin filaments, intermediate filaments), fluid (the cytosol) or dissolved species (such as ions, monomers, diverse proteins). Under the assumptions that the characteristic length-scale associated with each constituent is small compared to its size, a cell can be viewed as a multiphasic continuum that can be very well described within the framework of mixture theory. Since the objective of

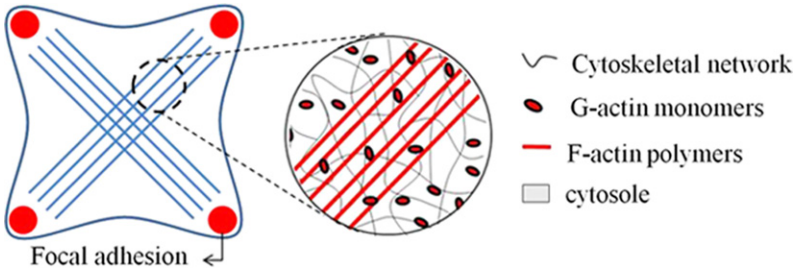

Fig. 1 – Illustration of the continuum formulation of the cell (Parker et al., 2008), decomposed into the cytoplasm and the cortical membrane. In the cytoplasm, a material point is seen as a mixture of four constituents, namely the passive cytoskeletal network, the contractile SF, the cytosol and dissolved G-actin monomers.

the present paper is to characterize the chemo-mechanical processes responsible for cell sensing and contraction, we propose to consider four constituents that are critical components of the contractile apparatus of a cell: (a) porous and passive cytoskeleton, made of a network of incompressible filaments and referred with the superscript s (as in solid), (b) an incompressible fluid representing the cytosol, referred with the superscript f (as in fluid), (c) dissolved globular actin monomers, referred by the superscript m (as in monomer) and (d) a network of contractile SF referred by the superscript p (as in polymer). The latter is the active constituent of the cytoskeleton. An illustration of this decomposition is given in Fig. 1. It should be noted that the notion of incompressibility is to be understood within the context of "homogenized equivalent constituents", this enables us to avoid complications associated with incompressible constituents in their natural state as described in Rajagopal and Tao (1995). The reasons for choosing these four constituents lie in the nature of chemo-mechanical processes responsible for contractility; SF (from actin monomers) are critical elements of contraction and the presence of the cytoskeleton must be included to assess cell deformation. In addition, the existence of the cytosol is essential for monomer transport and its mechanical function in resisting the cell's internal pressure.

Considering a planar cell (under plane stress conditions) as a closed domain Ω_0 delimited by a boundary Γ_0 in its initial configuration, one may locate a material point P by its position vector $\mathbf{X}$ in a Cartesian coordinate vector X_i, $i = 1, 2$. Upon deformation, at any time t, a material point associated with each constituent (represented by superscript $\alpha = s, f, m, p$) occupies a position $\mathbf{x}^\alpha$ defined by a continuous and differentiable function $\boldsymbol{\chi}^\alpha$ as:

$$\mathbf{x}^\alpha = \boldsymbol{\chi}^\alpha(\mathbf{X}, t). \tag{1}$$

The material derivative D^α/Dt following the motion of constituent α can then be introduced such that the velocity $\mathbf{v}^\alpha$ of each constituent is given as:

$$\mathbf{v}^\alpha = \frac{D^\alpha \mathbf{x}^\alpha}{Dt}. \tag{2}$$

Following these definitions, the relationship between spatial and material time derivatives for a continuous and differentiable function $A(\mathbf{x}, t)$ reads:

$$\frac{D^\alpha A}{Dt} = \frac{\partial A}{\partial t} + \nabla A \cdot \mathbf{v}^\alpha \tag{3}$$

where ∇ is the spatial gradient operator. In this paper, a Lagrangian viewpoint is adopted for the solid deformation while an Eulerian description is adopted for fluid flow and monomer transport. In other words, the solid skeleton is considered as a reference frame in which we compute motion and velocities. In this frame, we introduce relative velocities $\tilde{\mathbf{v}}^\alpha$ as:

$$\tilde{\mathbf{v}}^\alpha = \mathbf{v}^\alpha - \mathbf{v} \tag{4}$$

where $\mathbf{v} = \mathbf{v}^s$. We now make a fundamental assumption regarding material motion. As noted by Humphrey and Rajagopal in their treatise on growth (Humphrey and Rajagopal, 2002), there are many difficulties associated with the definition of mixture motion, as well as the partial stresses arising from different solid constituents. These issues result from the fact that based on the knowledge of mixture velocity, there exist a variety of ways to find the individual velocities of constituents. To circumvent this problem, we assume here that all solid constituents located at the same material point at time t follow the same motion. In other words, we assume that SF velocity is equal to the passive cytoskeleton velocity, or equivalently:

$$\tilde{\mathbf{v}}^p = \mathbf{0}. \tag{5}$$

This assumption enforces a constraint to the model as discussed in Humphrey and Rajagopal (2002), which motivates our appellation *"constraint mixture model"*. Furthermore since cell deformation is measured by the deformation of the passive cytoskeleton, it can be measured with the Green–Lagrange strain in the passive cytoskeleton:

$$\mathbf{E} = \frac{1}{2}(\mathbf{F}^T \cdot \mathbf{F} - \mathbf{I}), \qquad \mathbf{F} = \mathbf{F}^s = \frac{\partial \mathbf{x}}{\partial \mathbf{X}} \tag{6}$$

where $\mathbf{F}$ is the deformation gradient, $\mathbf{I}$ is the identity tensor and $\mathbf{x} = \mathbf{x}^s$. Finally, in order to follow the changes in cell constitution in time, we define the volume fraction ϕ^α, associated with each constituent representing the relative quantity of each constituent at a continuum point.

$$\phi^\alpha(\mathbf{x}, t) = \frac{V^\alpha}{V} \tag{7}$$

where V^α is unit volume of constituent α contained in a unit volume V of mixture at a material point $\mathbf{x}$ in the current configuration. Assuming that the cell is saturated with the four constituents, volume fractions satisfy the following relationship:

$$\sum_{\alpha=1}^{4} \phi^\alpha = \phi^s + \phi^f + \phi^m + \phi^p = 1 \tag{8}$$

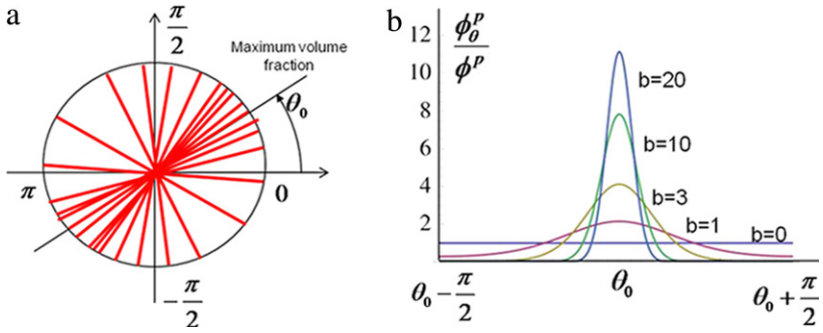

Fig. 2 – Illustration of SF volume fraction at a continuum point and its representation with a Von Mises distribution function.

at all times. A consequence of the above equation is that while the volume fraction of each constituent may change during cell deformation due to volume changes or mass exchange, their sum remains constant.

2.2. *Anisotropic SF distribution*

A particularity of the cell's internal structure is the presence of an evolving, strongly-oriented network of SF. For such anisotropic fibrous network, the volume fraction $\phi^p(\mathbf{x})$ does not provide sufficient information and the description needs to be enriched to account for the angular distribution of fibers. Concentrating on the case of a two-dimensional planar fibrous assembly in the neighborhood of a continuum point, the direction of an individual SF is designated by the angle θ measured between the fiber axis and the direction given by the base vector x_1. Based on this, a volume fraction ϕ^p_θ can be introduced as the ratio of the volume of fibers oriented in the θ-direction and the total volume. This gives rise to a distribution function ϕ^p_θ representing the variation in fiber density with direction, as shown in Fig. 2(a). In this paper, we propose to describe this distribution by the π-periodic Von Mises distribution function (which may be though of as a periodic version of the normal distribution) defined as Gasser et al. (2006):

$$\phi^p_\theta(\theta) = \phi^p \left(\frac{\exp[b\cos(2\theta - 2\theta_0)]}{I_0(b)} \right) \tag{9}$$

where $I_0(b)$ is the Bessel's function of the first kind of order zero defined as:

$$I_0(b) = \frac{1}{\pi}\int_0^\pi \exp(b\cos\theta)\mathrm{d}\theta. \tag{10}$$

The Von Mises distribution is represented in Fig. 2(b) when the largest fiber density is along the θ_0-direction. On the figure, it can clearly be seen that the parameter b in (9) captures the degree of anisotropy. In particular, when increasing b from 0 to ∞, the SF orientation varies from a totally isotropic distribution to a strongly oriented distribution in the direction $\theta = \theta_0$. To further simplify the formulation, the fiber distribution can be represented at a continuum point by a structure tensor $\mathbf{\Phi}^p$, a concept that was originally used to represent the evolution of the anisotropic structure of soft biological tissues during large deformations and remodeling (Menzel et al., 2008; Gasser et al., 2006). In a nutshell, this tensor is related to the fiber distribution ϕ^p_θ through a directional averaging operation $\langle\langle\bullet\rangle\rangle$ as follows:

$$\mathbf{\Phi}^p = \langle\langle \phi^p_\theta \mathbf{M}_\theta \rangle\rangle \quad \text{where } \langle\langle\bullet\rangle\rangle = \frac{1}{\pi}\int_{-\pi/2}^{\pi/2} \bullet\, \mathrm{d}\theta \tag{11}$$

where the matrix $\mathbf{M}_\theta$ is related to fiber direction vector $\mathbf{a} = [\cos\theta\ \sin\theta]^T$ by:

$$\mathbf{M}_\theta = \mathbf{a}\otimes\mathbf{a} = \begin{bmatrix} \cos^2\theta & \cos\theta\sin\theta \\ \cos\theta\sin\theta & \sin^2\theta \end{bmatrix}. \tag{12}$$

From this definition, one can show that the structure tensor $\mathbf{\Phi}^p$ is symmetric and is related to the total volume fraction ϕ^p of SF appearing in (8) by:

$$\phi^p = \langle \phi^p_\theta \rangle = \mathrm{tr}(\mathbf{\Phi}^p) \quad \text{where } \langle\bullet\rangle = \frac{1}{\pi}\int_{-\pi/2}^{\pi/2} \bullet\, \mathrm{d}\theta. \tag{13}$$

Here, we introduced the averaging operation $\langle\bullet\rangle$ that relates the total volume fraction of SF to the volume fraction in specific directions. It is particularly useful to realize that, for a two-dimensional distribution, the symmetry of $\mathbf{\Phi}^p$ implies that it can be represented in terms of three independent variables $\{\phi^p, \eta, \theta_0\}$, where η refers to the degree of anisotropy and θ_0 shows the principal direction of SF. In this context, the structure tensor may be constructed in the form:

$$\mathbf{\Phi}^p = \phi^p[\eta\mathbf{I} + (1-2\eta)\mathbf{M}_{\theta_0}] \tag{14}$$

where $\mathbf{I}$ is the identity tensor and the matrix $\mathbf{M}_{\theta_0}$ was defined in (11). It can be seen that if $\eta = 0$, all fibers are aligned in the same direction (defined by angle θ_0), whereas as $\eta \to 1/2$, the distribution becomes isotropic. Because of their similar physical interpretation, it is possible to find a relationship between parameters b (appearing in the Von Mises distribution) and η by substituting (9) into (14). One can show that:

$$\eta = \frac{1}{\pi}\int_{-\pi/2}^{\pi/2} \frac{\exp[b\cos(2\theta)]\sin^2\theta}{I_0(b)}\mathrm{d}\theta. \tag{15}$$

This integral may be computed numerically to determine the b/η curve as shown in Fig. 3(b). This ensures that there is a one-to-one mapping between the structure tensor shown in (14) and the Von Mises distribution (9).

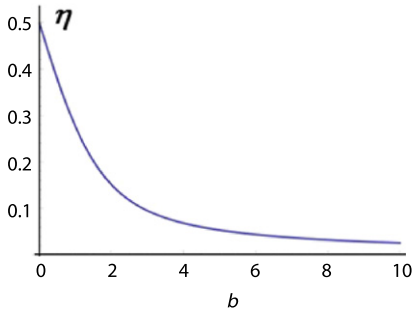

Fig. 3 – Relationship between parameters b and η.

3. Mass transport and mass exchange

Cell contractility relies on the mass exchange through the polymerization of G-actin monomers into actin filaments that are a key structural component of SF. These reactions are possible through the transport of G-actin monomers to the site of reaction, a process that depends on the combination of cytosol flow and G-actin diffusion (Engelke et al., 2010). The present section discusses the mathematical description of these phenomena.

3.1. Mass balance of individual constituents

To accurately describe mass transport and mass transfer, it is essential to ensure that mass is conserved throughout the process of cell contraction. In this context, let us introduce an effective density that represents the mass of the αth constituent per unit volume of mixture as follows:

$$\rho^\alpha = \phi^\alpha \rho_r^\alpha \quad \alpha = s, f, m \tag{16}$$

$$\rho_\theta^\alpha = \phi_\theta^\alpha \rho_r^\alpha \quad \alpha = p \tag{17}$$

where ρ_r^α is the real density of constituent α. A particularity of the present approach is the description of the anisotropic SF distribution through the direction dependent mass density ρ_θ^p. As we will see below, this definition is an important feature of the model as it enables a natural description of the evolution of SF evolution through the mass balance equation. Thus, in the presence of mass exchange between constituents, the conservation of mass for each constituent is written in terms of mass source (or sink) term $\rho_r^\alpha \Gamma^\alpha$ that represents the rate of added mass to the $\alpha - th$ component per current volume. In the particular case of incompressible constituents (i.e., the real densities ρ_r^α are constant in time and space), we can write:

$$\rho_r^\alpha \frac{\partial \phi^\alpha}{\partial t} + \rho_r^\alpha \nabla \cdot (\phi^\alpha \mathbf{v}^\alpha) = \rho_r^\alpha \Gamma^\alpha \quad \alpha = s, f, m \tag{18}$$

$$\rho_r^\alpha \frac{\partial \phi_\theta^\alpha}{\partial t} + \rho_r^\alpha \nabla \cdot (\phi_\theta^\alpha \mathbf{v}^\alpha) = \rho_r^\alpha \Gamma_\theta^\alpha \quad \alpha = p \tag{19}$$

where the second equation represents the evolution of SF density in certain direction (denoted as θ). In particular, the quantity Γ_θ^α denotes the rate of SF polymerization (if positive) or depolymerization (if negative). Writing the above equations with respect to the cytoskeleton motion, we obtain:

$$\frac{D\phi^\alpha}{Dt} + \phi^\alpha \nabla \cdot \mathbf{v} + \nabla \cdot (\phi^\alpha \tilde{\mathbf{v}}^\alpha) = \Gamma^\alpha \quad \alpha = s, f, m \tag{20}$$

$$\frac{D\phi_\theta^\alpha}{Dt} + \phi_\theta^\alpha \nabla \cdot \mathbf{v} + \nabla \cdot (\phi_\theta^\alpha \tilde{\mathbf{v}}^\alpha) = \Gamma_\theta^\alpha \quad \alpha = p \tag{21}$$

where we used the material time derivative $D/Dt = D^\alpha/Dt$ with respect to the cytoskeleton following (3). Following the directional averaging operation defined in the previous section and applying it to each term in (21), the balance of mass for SF can be written in the following tensorial form

$$\frac{D\mathbf{\Phi}^p}{Dt} + \mathbf{\Phi}^p \nabla \cdot \mathbf{v} = \mathbf{\Gamma}^p \quad \text{where } \mathbf{\Gamma}^p = \langle\langle \Gamma_\theta^p \rangle\rangle \tag{22}$$

and we used the fact that $\tilde{\mathbf{v}}^p = 0$. The tensor $\mathbf{\Gamma}^p$ can be interpreted as the anisotropic rate of mass creation of SF per unit volume at time t. Similarly to the structure tensor $\mathbf{\Phi}^p$, the maximum and minimum rates of F-actin formation are the largest and smallest eigenvalues of $\mathbf{\Gamma}^p$, while their directions are given by the eigenvectors of $\mathbf{\Gamma}^p$. To describe the transport of cytosol and G-actin monomers, one can also introduce the flux:

$$\mathbf{J}^\alpha = \phi^\alpha \tilde{\mathbf{v}}^\alpha \quad \alpha = f, m \tag{23}$$

such that the final system of equations describing the mass balance of solid (cytoskeleton), fluid (cytosol), G-actin monomers and SF, respectively reads:

$$\frac{D\phi^s}{Dt} + \phi^s \nabla \cdot \mathbf{v} = 0 \tag{24}$$

$$\frac{D\phi^f}{Dt} + \nabla \cdot \mathbf{J}^f + \phi^f \nabla \cdot \mathbf{v} = 0 \tag{25}$$

$$\frac{D\phi^m}{Dt} + \nabla \cdot \mathbf{J}^m + \phi^m \nabla \cdot \mathbf{v} = \Gamma^m \tag{26}$$

$$\frac{D\mathbf{\Phi}^p}{Dt} + \mathbf{\Phi}^p \nabla \cdot \mathbf{v} = \mathbf{\Gamma}^p. \tag{27}$$

It is also important to mention that the total mass balance of SF (averaged over all directions) is found by considering the trace of (27), i.e.

$$\frac{D\phi^p}{Dt} + \phi^p \nabla \cdot \mathbf{v} = \Gamma^p. \tag{28}$$

3.2. Mass balance of the mixture

The mass conservation of the mixture is typically determined by adding the various contributions from each constituent. Summing equations (24)–(26) and (28), we obtain:

$$\nabla \cdot \mathbf{J}^f + \nabla \cdot \mathbf{J}^m + \nabla \cdot \mathbf{v} = \Gamma^m + \Gamma^p. \tag{29}$$

Assuming that no mass is added to the cell during the contraction process, the total mass creation (or loss) for the mixture should vanish. This enables us to write the following relation:

$$\sum_\alpha \rho_r^\alpha \Gamma^\alpha = \rho_r^p \Gamma^p + \rho_r^m \Gamma^m = 0. \tag{30}$$

Assuming that the real densities of actin are the same in its monomer and polymer form ($\rho_r^m = \rho_r^p$), the mass equation for the mixture finally becomes:

$$\nabla \cdot \mathbf{J}^f + \nabla \cdot \mathbf{J}^m + \nabla \cdot \mathbf{v} = 0. \tag{31}$$

3.3. Mass transport through the cytoskeleton

Mass transport within the cytoplasm is an important player in both the passive mechanical response of cells and the dynamics of cell contraction. For instance, mechanical testing

procedures, such as micropipette aspiration, clearly exhibit a time-dependency that is usually attributed to a combination of the intrinsic visco-elasticity of the cytoskeleton and the flow driven deformation of the cytoplasm. In terms of cell morphology, it is likely that cytosol flow governs the number and size of cell protrusions. Indeed, Weiss and Garber (1952), in his analysis on the shape of mesemchymal cells, explained the development of cell extensions (or filopodia) in terms of competitive mechanisms based on the amount of cytosol each protrusion could intake. Complex interactions may exist between the transport and fluid and that of dissolved species, which may result in a quite complex problem. However, it is important to make a few simplifying assumptions for the sake of clarity. The present analysis is then based on the following points. First, assuming that the concentration of G-actin in the cytosol is small, it is reasonable to say that actin monomer transport does not affect the interstitial flow of cytosol. In other words, cytosol flow can be expressed only in terms of a differential of pressure though Darcy's law as follows:

$$\mathbf{J}^f = -\frac{\mathbf{K}}{\mu}\cdot\nabla p \tag{32}$$

where $\mathbf{K}$ is the permeability tensor that depends on the porosity and anisotropy of the cytoskeleton and μ is the dynamic viscosity of the cytosol. Further assuming that the anisotropy of SF does not affect the permeability (this assumption can be relaxed in a future study), an isotropic permeability κ is considered such that $\mathbf{K} = \kappa\mathbf{I}$, where $\mathbf{I}$ is the identity tensor. In addition, the transport of G-actin monomers is assumed to arise from two mechanisms: (a) convection with the cytosol and (b) diffusion through the cytosol with a diffusion coefficient D. One can therefore write:

$$\mathbf{J}^m = -\frac{\phi^m}{\phi^f}\frac{\kappa}{\mu}\nabla p - \phi^f D\nabla\left(\frac{\phi^m}{\phi^f}\right). \tag{33}$$

This above relationship implicitly assumes that there are no interactions between G-actin monomers and the cytoskeleton, an assumption that is reasonable with the small relative size of G-actin monomers compared to cytoskeleton mesh-size. Eq. (33) shows that the diffusion constant D has a role in controlling the rate of cell contractility by providing more or less resistance to the flux of monomers towards the site of SF polymerization.

3.4. *Mass exchange and SF formation*

Actin polymerization and SF formation are anisotropic processes that strongly depend on the level of contractile stress in existing SF. The rate of SF polymerization Γ_θ is therefore derived based on the following assumptions: (a) the chemical reaction between G-actin and F-actin is described by a first-order kinetic equation and (b) *the rate of SF formation is affected by the magnitude of contractile stress* T^p_θ *in direction* θ. The latter statement is the main assumption of this paper and will be shown to be responsible for the mechano-sensitivity of cell contraction. The rate equation describing the chemical equilibrium of SF is then written in terms of rates of formation k^f and dissociation k^d of F-actin as:

$$\Gamma^p_\theta = \frac{M^a}{\rho^a}(k^f c^m - k^d c^p_\theta) \quad \text{where } k^f = k^f(T^p_\theta) \tag{34}$$

where M^a and ρ^a are the molar mass and real density of actin, assumed to be the same in its polymer (p) and monomer (m) configuration. Furthermore, the concentrations c^p_θ and c^m are related to the respective volume fractions of SF and G-actin monomers by:

$$c^p_\theta = \frac{\rho^a}{M^a}\phi^p_\theta \quad \text{and} \quad c^m = \frac{\rho^a}{M^a}\frac{\phi^m}{\phi^f+\phi^m} \approx \frac{\rho^a}{M^a}\frac{\phi^m}{\phi^f}. \tag{35}$$

Note that the concentration of F-actin is taken as the number of moles per unit volume of mixture while the concentration of G-actin is the number of moles of G-actin per unit volume of cytosol-G actin mixture. To characterize the rise in SF polymerization with contractile stress T^p_θ, we introduce a linear approximation of the function $k^f(T^p_\theta)$ appearing in (34) as:

$$k^f(T^p_\theta) = k^f_0 + k^f_1 T^p_\theta \tag{36}$$

where the constant k^f_0 denotes the rate of F-actin formation in the absence of contractile stress and $k^f_1 > 0$ measures the increase in polymerization rate with contraction T^p_θ. Combining the definition of the SF production tensor (22) with Eqs. (34) and (36), and using (35), it is possible to derive the following expression for $\mathbf{\Gamma}^p$:

$$\mathbf{\Gamma}^p = \langle\langle \Gamma^p_\theta \rangle\rangle = \left(\frac{1}{2}k^f_0\mathbf{I} - k^f_1\mathbf{T}^p\right)\frac{\phi^m}{\phi^f} - k^d_0\mathbf{\Phi}^p \tag{37}$$

where the contractile stress $\mathbf{T}^p$ from SF is defined as the directional average of the contractions stress T^p_θ from individual SF as:

$$\mathbf{T}^p = \langle\langle T^p_\theta \rangle\rangle. \tag{38}$$

Eq. (37) is a critical component of the proposed model as it describes the evolution of SF concentration and distribution in the cell in terms of the level of contractile stress. Indeed, combining (27) and (37), the following evolution equation is obtained for $\mathbf{\Phi}^p$

$$\frac{D\mathbf{\Phi}^p}{Dt} = \underbrace{\left(\frac{1}{2}k^f_0\mathbf{I} + k^f_1\mathbf{T}^p\right)\frac{\phi^m}{\phi^f}}_{\text{force dependent formation}} - \underbrace{k^d_0\mathbf{\Phi}^p}_{\text{dissociation}} - \underbrace{\mathbf{\Phi}^p\nabla\cdot\mathbf{v}}_{\text{volume change}}. \tag{39}$$

This expression clearly shows that SF formation in various directions depends on the availability of actin monomers (through ϕ^m), the concentration of existing SF (through $\mathbf{\Phi}^p$) and the level of contractile force (through $\mathbf{T}^p$). Finally, the last term in (39) characterizes the change in fiber concentration with volumetric deformation of the cell (through the term $\nabla\cdot\mathbf{v}$).

4. Force generation and mechanical equilibrium

The generation of active forces by SF plays a significant role in the process of mechano-sensing and cell deformation. Indeed, mechanical force and resulting deformation play two major roles in cell contraction. First, as seen in (39), mechanical stress induces SF formation, which directly affects the magnitude of contraction. Second, because SF

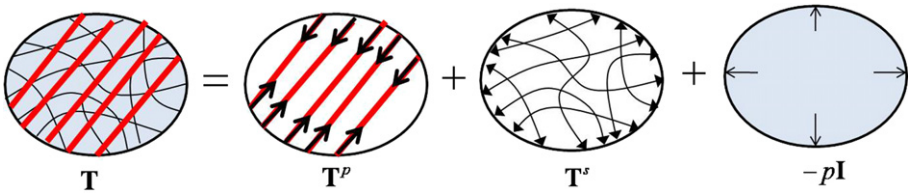

Fig. 4 – Decomposition of the Cauchy stress.

possess a sarcomeric structure similar to that found in myofibrils of muscle cells, contractile forces are very likely to be highly dependent on the strain-rate and current length of SF, as predicted by cross-bridge dynamics models (Carlson and Wilkie, 1974). To incorporate these mechanisms into the proposed model, this section concentrates on key mechanical aspects of the problem by (a) writing the force equilibrium between the four constituents present in the cell and (b) introducing constitutive relations for SF contraction and cytoskeleton deformation.

4.1. *Mechanical equilibrium of the cell*

Let us first consider the mechanical equilibrium of the cell by writing the balance of momentum associated with each constituent. Introducing $\mathbf{T}^\alpha$ as the partial Cauchy stress associated with constituent α, the momentum balance for each constituent can be written (Coussy, 2004):

$$\rho^\alpha \frac{\mathrm{D}^\alpha \mathbf{v}^\alpha}{\mathrm{Dt}} = \nabla \cdot \mathbf{T}^\alpha + \rho^\alpha \mathbf{b} + \mathbf{f}^\alpha \tag{40}$$

where $\mathbf{b}$ is the external force per unit mass of constituent α and $\mathbf{f}^\alpha$ represents forces (per unit volume) acting on constituent α due to its interactions with other constituents. Assuming that at the mixture level, the net force resulting from interactions between constituent must vanish, the following equality must hold:

$$\sum_{\alpha=1}^{4} \mathbf{f}^\alpha = \mathbf{0}. \tag{41}$$

Furthermore, due to the slow time scales associated with cell motion, inertial forces on each constituent may be neglected; this implies that the left hand term in (40) can be neglected. The equilibrium of the mutiphasic mixture can then be obtained by adding the contributions (40) from each constituent; this yields the following form:

$$\nabla \cdot \mathbf{T} + \rho \mathbf{b} = 0 \tag{42}$$

where the total Cauchy stress $\mathbf{T}$ contains a contribution from each constituent (Fig. 4):

$$\mathbf{T} = \sum_{\alpha=1}^{4} \mathbf{T}^\alpha = \mathbf{T}^s + \mathbf{T}^f + \mathbf{T}^m + \mathbf{T}^p. \tag{43}$$

Here, $\mathbf{T}^s$ may be interpreted as the passive stress arising from cyoskeleton deformation, $\mathbf{T}^p$ is the contractile stress exerted by SF and $\mathbf{T}^f$ results from the pressurization of the cytosol such that

$$\mathbf{T}^f = -\phi^f p \mathbf{I} \tag{44}$$

where p is the cytosol pressure. In this study, the partial pressure $\mathbf{T}^m$ due to the presence of G-actin monomers is neglected because of the low concentration of G-actin monomomers in the cytosol. It is also important to mention that since each constituent verifies the balance of angular momentum, partial stresses $\mathbf{T}^\alpha$ (and therefore $\mathbf{T}$) are symmetric tensors.

4.2. *Active contraction of SF*

Let us discuss the contractile stress $\mathbf{T}^p$ originating from the tension developed in SF through acto-myosin interactions. Noting that there are strong similarities between the sarcomeric structure of SF and that of myofibriles (in myocytes), one may borrow the extensive body of knowledge on the mechanics of cross-bridge models describing acto-myosin contraction in muscle cells. Considering a one-dimensional SF undergoing contraction, the developed force T is known to be dependent of two quantities: the change of fiber length (the relationship is known as the length–tension relationship Carlson and Wilkie, 1974) and the rate of change of fiber length (known as the velocity–tension relation Hill, 1938). In this work, we introduce a model describing the uniaxial contractile stress T^p in fibers in terms of their normal strain ϵ (measuring the change in fiber length) and strain-rate $\dot{\epsilon}$ (measuring the rate of fiber shortening during contraction). In general, the tension T^p can be written in the form:

$$\frac{T^p}{\bar{T}} = T^\star(\epsilon, \dot{\epsilon}) \tag{45}$$

where $\bar{T}$ is the isometric contraction associated with a single SF in its original length ($\epsilon = 0$) and a vanishing strain rate ($\dot{\epsilon} = 0$). In other words, the function $T^\star$ verifies the equality $T^\star(0,0) = 1$. The derivation of function $T^\star$ is now presented based on conventional knowledge of sarcomere contraction.

Length–tension relation. The length–tension relation describes a drop in active acto-myosin contraction T as the length of sarcomere deviates from its original value. Consistent with the prediction from the sliding filament theory, sarcomeres exert the highest contractile stress T when $\epsilon = 0$ (or $\ell = \ell_0$) and this force decreases in a nonlinear fashion as the strain deviates from 0, either in a positive or negative manner.

Remark. Note that because SFs form at different times, they are usually characterized by different natural configurations (or stress-free state) (Na et al., 2007). Since the change of length of a single SF is measured with respect to its natural configuration, the tension $T^\star$ cannot generally be measured in terms of ϵ. In the present approach, it is assumed that SF formation occurs in a way such that their natural configuration is the same at that of the cytoskeleton and thus the strain ϵ is a good measure of change in length. While this assumption has been applied as a mean to simplify

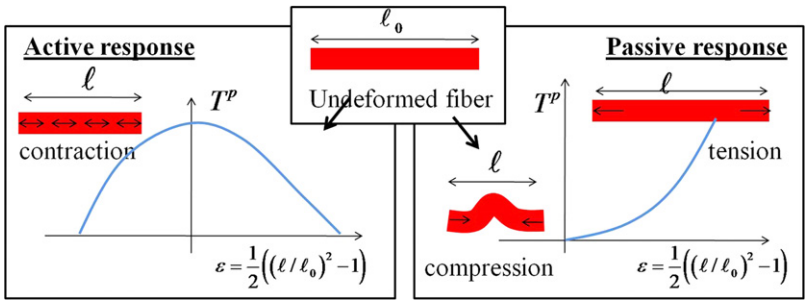

Fig. 5 – Active and passive response of a SF. The uniaxial contractile stress is T^p and the normal strain is a function of the ratio of the final fiber length and initial fiber length l0.

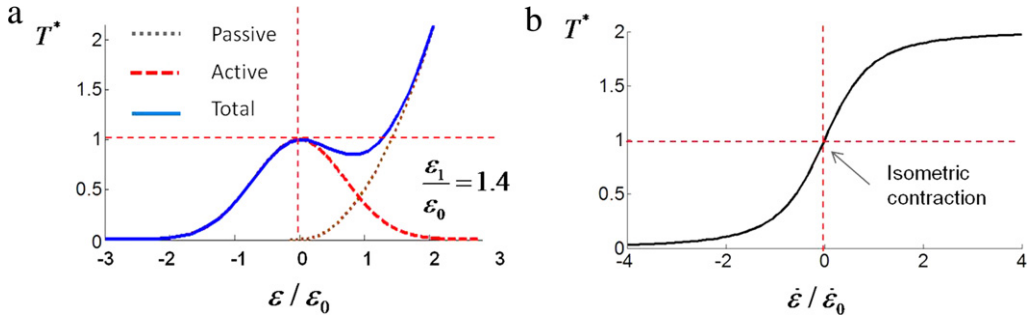

Fig. 6 – (a) Strain-tension relationship $f(\epsilon)$ and (b) strain-rate tension relationship $g(\dot{\epsilon})$ are used in the study to capture the length and velocity–tension relation, respectively, observed in muscle cells.

the proposed model, it can be relaxed in future studies by computing the stress from new SF in terms of a time integral as suggested by Humphrey and Rajagopal in Humphrey and Rajagopal (2002).

Furthermore, when stretched, SFs develop a passive stress that acts in a similar way cables resist tension. However, because resistance in compression is negligible as fibers become slack, the passive behavior of SF is described as follows: (a) for negative strains, passive stress is zero and (b) for tensile strain, SFs exhibit a strain hardening response. The active and passive response of SF is summarized in Fig. 5. Considering the case of isometric tension ($\dot{\epsilon} = 0$), the change of tensile stress in a SF is written:

$$T^\star(\epsilon, 0) = f(\epsilon) \quad \text{where } f(\epsilon) = \begin{cases} e^{-\left(\frac{\epsilon}{\epsilon_0}\right)^2} & \text{if } \epsilon < 0 \\ e^{-\left(\frac{\epsilon}{\epsilon_0}\right)^2} + \left(\frac{\epsilon}{\epsilon_1}\right)^2 & \text{if } \epsilon \geq 0 \end{cases} \tag{46}$$

where the constant ϵ_0 describes how quickly contraction decreases as strain deviates from zero and ϵ_1 characterizes the passive strain hardening of SF. Note that the above function is such that $f(0) = 1$, in order to satisfy the fact that $T^\star(0, 0) = 1$. Fig. 6(a) shows the relationship between $T^\star$ and scaled strain ϵ/ϵ_0 considered in the proposed model (in the case of isometric tension).

Velocity–tension relation. The rate at which a fiber shortens is also known to affect the magnitude of the contractile force. Typically, contraction declines in a hyperbolic fashion as the rate of shortening increases ($\dot{\epsilon} < 0$) and ultimately vanishes for very high rates of shortening (Hill, 1938). However, as a sarcomere lengthens ($\dot{\epsilon} > 0$), it is found that contraction increases and reaches a value well above the isometric tension for high values of positive strain rate. To characterize this behavior, we introduce a function g that describes the change in contraction T with strain rate in the particular case of a vanishing strain ϵ (i.e., the fiber length is the initial length ℓ_0)

$$T^\star(0, \dot{\epsilon}) = g(\dot{\epsilon}) = 1 + \frac{\dot{\epsilon}/\dot{\epsilon}_0}{\sqrt{(\dot{\epsilon}/\dot{\epsilon}_0)^2 + 1}}. \tag{47}$$

As seen in Fig. 6(b), function g is antisymmetric and verifies the following criteria: (a) $g \to 0$ as $\epsilon \to -\infty$, (b) $g \to 2$ as $\epsilon \to +\infty$ and (c) $g(0) = 1$. In other words, the maximum contractile stress that can be developed by the fiber is twice the isometric tension $\bar{T}$. Literature on muscle mechanics (Carlson and Wilkie, 1974) has shown that in reality, the force-velocity curve is not exactly antisymmetric but this aspect does not affect the main concepts presented in this paper.

Uni-directional model of fiber contraction. While the above models are proposed at constant strain rate or constant strain, respectively, in general, fiber contraction is affected by both fiber strain and its rate simultaneously. Assuming that the effects of strain and strain rate on fiber tension are completely independent, it is possible to derive a general model that defines $T^\star$ as the product of functions f and g defined in (46) and (47). This yields:

$$T^\star(\epsilon, \dot{\epsilon}) = f(\epsilon) g(\dot{\epsilon}) = \begin{cases} \left(1 + \frac{\dot{\epsilon}/\dot{\epsilon}_0}{\sqrt{(\dot{\epsilon}/\dot{\epsilon}_0)^2 + 1}}\right) e^{-\left(\frac{\epsilon}{\epsilon_0}\right)^2} & \text{if } \epsilon < 0 \\ \left(1 + \frac{\dot{\epsilon}/\dot{\epsilon}_0}{\sqrt{(\dot{\epsilon}/\dot{\epsilon}_0)^2 + 1}}\right) \left(e^{-\left(\frac{\epsilon}{\epsilon_0}\right)^2} + \left(\frac{\epsilon}{\epsilon_1}\right)^2\right) & \text{if } \epsilon \geq 0. \end{cases} \tag{48}$$

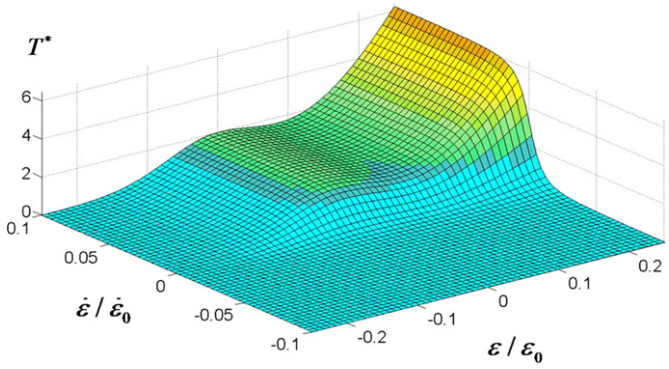

Fig. 7 – Three-dimensional representation of the cell contraction $T^\star$ as a function of SF strain ϵ/ϵ_0 and strain rate $\dot{\epsilon}/\dot{\epsilon^0}$.

We give a three-dimensional representation of contraction in terms of ϵ and $\dot{\epsilon}$ in Fig. 7.

Contraction of the SF network. The above model is able to characterize the contraction of a single SF but does not describe the contraction of an anisotropic network. This issue can be addressed by relating the contraction of a single SF to the contractile stress tensor $\mathbf{T}^p$, as follows. First, we write the uniaxial contractile stress T^p_θ in a specific direction θ in terms of the volume fraction of SF and the stress $T = \bar{T}T^\star$ in each individual fiber as:

$$T^p_\theta = \phi_\theta \bar{T} T^\star. \tag{49}$$

Second, the stress tensor $\mathbf{T}^p$ is derived from the averaging equation defined in (38): $\mathbf{T}^p = \langle\langle T^p_\theta \rangle\rangle$. Referring to the definition of the averaging operation (12), the stress $\mathbf{T}^p$ can then be found in terms of the Green–Lagrange strain tensor $\mathbf{E}$ and its material time derivative $\dot{\mathbf{E}}$ by computing the integral:

$$\mathbf{T}^p(\mathbf{E}, \dot{\mathbf{E}}) = \frac{\bar{T}}{\pi} \int_{-\pi/2}^{\pi/2} \phi^p_\theta T^\star(\epsilon_\theta, \dot{\epsilon}_\theta) \mathbf{M}_\theta \mathrm{d}\theta \tag{50}$$

where $\epsilon_\theta = \mathbf{E} : \mathbf{M}_\theta$ and $\dot{\epsilon}_\theta = \dot{\mathbf{E}} : \mathbf{M}_\theta$.

Here, we used the fact that the tensile strain (and its rate) in a certain direction can be found through a double tensor contraction ":" with the matrix $\mathbf{M}_\theta$. The above integral can be determined computationally using the Von Mises distribution and the state of strain and strain rate at a material point. Relation (50) therefore clearly establishes a link between contractile stress, fiber distribution and the underlying molecular mechanisms of the cross-bridge dynamics.

4.3. *Cytoskeleton elasticity*

According to the velocity–tension relation, it is clear that contractility is promoted by a scenario in which the rate of SF shortening is limited. There are two elements that contribute to the resistance of contractile deformation: the passive cytoskeleton and the underlying substrate (through cell-matrix attachments provided by focal adhesions). The passive cytoskeleton consists of a filamentous network that can resist actin contraction through the mechanical balance between compressive elements (microtubules), tensile elements (actin and intermediate filaments) and cytosol pressure. These contributions should be accounted for in the description of the cytoskeleton stress $\mathbf{T}^s$ through the constitutive relation. According to the effective stress principle (Coussy, 2004), this stress is decomposed into pressure and an effective stress $\mathbf{T}^s_e$ carried by the dry cytoskeleton as follows:

$$\mathbf{T}^s = -\phi^s p \mathbf{I} + \mathbf{T}^s_e(\mathbf{E}). \tag{51}$$

Assuming an isotropic passive cytoskeleton, the effective stress can be related to deformation $\mathbf{E}$ through an isotropic, linear elastic relation. More complex behavior of the cytoskeleton (including its known nonlinear visco-elastic response) may be added to the present model in future studies. Concentrating on a simple hypo-elastic constitutive behavior, an objective rate of the effective stress $\mathbf{T}^{\sigma J}_e$ is written

$$\mathbf{T}^{\sigma J}_e = \mathbf{C}^{\sigma J} : \mathbf{D} \tag{52}$$

where the rate of deformation is given by $\mathbf{D} = \mathbf{F}^{-T} \cdot \dot{\mathbf{E}} \cdot \mathbf{F}^{-1}$, $\mathbf{F}$ is the deformation gradient and a superposed dot refers to the material time derivative with respect to cytoskeleton motion. For an isotropic flimentous network, the fourth-order elastic matrix $\mathbf{C}^{\sigma J}$ is written in terms of the Lame constants λ and μ as:

$$C^{\sigma J}_{ijkl} = 2(\mu - \lambda \ln J)\delta_{ik}\delta_{jl} + \lambda \delta_{ij}\delta_{kl} \tag{53}$$

where δ is the Kronecker delta. The above matrix can be rewritten in terms of the Young's modulus $E = \mu(3\lambda + 2\mu)/(\lambda + \mu)$ that can generally be measured from mechanical testing of cell deformation. It is also important to mention that while the material response of the cytoskeleton is based on linear assumptions, the relation between force and displacement is nonlinear due to geometrical effects associated with finite deformation.

5. Model prediction

In this section, we propose using the multi-physics model to investigate the behavior of cells and their interaction with an external mechanical environment (or support). We are particularly interested in understanding how cell contraction and force generation is affected by the stiffness of the support as predicted by experiments. For this, we consider two situations: (a) the case of homogeneous contraction of a square cell and (b) the case of a square cell supported by elastic springs at its four corners.

Table 1 – Parameters used in the simulations.

Definition	Symbol	Value	Unit	Reference
Cytosol volume fraction	ϕ^c	70	%	Ateshian et al. (2006)
Cytoskeleton volume fraction	ϕ^s	25	%	n/a
F + G actin volume fraction	$\phi^m + \phi^p$	5	%	n/a
Rate of SF formation	k_0^f	0.0001	s^{-1}	Rubinstein et al. (2005)
Mechano-sensitive rate of SF formation	k_1^f	0.05	s^{-1}	Rubinstein et al. (2005)
Rate of SF dissociation	k_0^d	0.1	s^{-1}	Rubinstein et al. (2005)
Cytoskeleton permeability	κ/μ	$1 \cdot 10^{-15}$	$m^4/N\,s$	Guilak and Mow (2000)
G-actin diffusion constant	D	$1 \cdot 10^{-5}$	m^2/s	Rubinstein et al. (2005)
Young's modulus	E	70	Pa	Deshpande et al. (2006)
Poisson's ratio	ν	0.3		Deshpande et al. (2006)
Fiber maximum tensile stress	$\bar{T}$	20 000	Pa	White and Fujiwara (1986); Kumar et al. (2006); Tsuda et al. (1996)
Model constant	$\dot{\varepsilon}_0$	0.01	s^{-1}	Deshpande et al. (2006)
Model constant	ε	0.1		Carlson and Wilkie (1974)
F/G molar mass ratio	M^p/M^m	100		n/a
F/G true density ratio	ρ_R^p/ρ_R^m	1		n/a

5.1. *Non-dimensionalization and solution strategy*

Before assessing the physical behavior of the system, we recognize that the above model possesses a certain number of parameters, whose respective role in the cell's behavior may be challenging to assess. To simplify the approach, one can scale these parameters with respect to characteristic time, dimension and force that are inherent to cellular systems. Let $t_0 = 1/\dot{\epsilon}_0$, ℓ_0 and $T_0 = \bar{T}$ be the scales of time, length and force, respectively. The non-dimensional variables (denoted with the superscript "$\star$") are then defined as:

$$t^\star = \frac{t}{t_0} = \dot{\epsilon}_0 t \qquad \mathbf{x}^\star = \frac{\mathbf{x}}{\ell_0} \qquad \mathbf{T}^{\alpha\star} = \frac{\mathbf{T}^\alpha}{T_0} = \frac{\mathbf{T}^\alpha}{\bar{T}} \tag{54}$$

$$\mathbf{v}^\star = \frac{\mathbf{v}}{\dot{\epsilon}_0 \ell_0} \qquad \dot{\mathbf{E}}^\star = \frac{\dot{\mathbf{E}}}{\dot{\epsilon}_0} \qquad p^\star = \frac{p}{\bar{T}} \qquad \mathbf{J}^{\alpha\star} = \frac{\mathbf{J}^\alpha}{\dot{\epsilon}_0 \ell_0 c_0}. \tag{55}$$

In addition, the non-dimensional material parameters (diffusion coefficient, permeability, cytosol viscosity, stiffness and rate constants) are given by:

$$D^\star = \frac{D}{\dot{\epsilon}_0 \ell_0^2} \qquad \kappa^\star = \frac{\kappa}{\ell_0^2} \qquad \mu^\star = \frac{\dot{\epsilon}_0}{\bar{T}}\mu \qquad \mathbf{C}^\star = \frac{\mathbf{C}}{\bar{T}} \tag{56}$$

$$k^{d\star} = \frac{k^d}{\dot{\epsilon}_0} \qquad k_0^{f\star} = \frac{k_0^f}{\dot{\epsilon}_0} \qquad k_1^{d\star} = \frac{\bar{T}}{\dot{\epsilon}_0} k_1^d. \tag{57}$$

The physical state of a material point in the cell is determined by the four following fields: the non-dimensional velocity $\mathbf{v}^\star$, cytosol pressure $p^\star$, fraction of G-actin monomers $\phi^{m\star}$ and SF structure tensor $\mathbf{\Phi}^{p\star}$. These fields are solutions of the system of coupled non-dimensional partial differential equations derived in this paper that consists of (a) momentum balance (40), (b) mixture mass balance (31), (c) cytosol mass balance (25) and (d) mass balance of SF (27) as follows:

$$\nabla^\star \cdot (\mathbf{T}^{s\star} + \mathbf{T}^{p\star} - p^\star \mathbf{I}) = \mathbf{0} \tag{58}$$

$$\frac{D\phi^{f\star}}{Dt^\star} - \frac{\kappa^\star}{\mu^\star}\nabla^{\star 2} p^\star + \phi^{f\star}\nabla^\star \cdot \mathbf{v}^\star = 0 \tag{59}$$

$$-\frac{\kappa^\star}{\mu^\star}[(1 + c^m)\nabla^{\star 2} p^\star + \nabla^\star c^m \cdot \nabla^\star p^\star] - D^\star \nabla^\star \cdot (\phi^{f\star}\nabla c^m) + \nabla^\star \cdot \mathbf{v}^\star = 0 \tag{60}$$

$$\frac{D\mathbf{\Phi}^{p\star}}{Dt^\star} - \left(\frac{1}{2}k_0^{f\star}\mathbf{I} + k_1^{f\star}\mathbf{T}^{p\star}\right)\frac{\phi^m}{\phi^f} + (k_0^{d\star} + \nabla^\star \cdot \mathbf{v}^\star)\mathbf{\Phi}^{p\star} = \mathbf{0} \tag{61}$$

where the constitutive relation for cytosol and monomer transport were used and $\phi^m = \frac{M^a}{\rho^a}\phi^f c^m$. Boundary conditions must be applied in order to describe the applied traction $\mathbf{t}^e$ on the cell boundary (written in terms of the total stress $\mathbf{T}$) and ensure that there is no flux of cytosol and actin monomers across the cell membrane Γ:

$$\mathbf{T} \cdot \mathbf{n} = \mathbf{t}^e, \qquad \mathbf{j}^f \cdot \mathbf{n} = 0, \qquad \mathbf{j}^m \cdot \mathbf{n} = 0 \tag{62}$$

where $\mathbf{n}$ denotes the outward unit vector to Γ. These equations can be solved using a nonlinear implicit finite element formulation, the details of which will be introduced in a companion paper (Farsad and Vernerey, in preparation). Finally, simulation results shown in the next section were obtained using the parameters shown in Table 1. Regarding model constants, the isometric contractile force and cross-sectional area of SF are estimated to be around 600 pN (Tsuda et al., 1996) and 0.03 μm^2 (White and Fujiwara, 1986; Kumar et al., 2006), respectively. The isometric stress($\bar{T}$) can therefore be calculated to be on the order 20 000 Pa (which is the value chosen in our simulations).

5.2. *Homogeneous cell contraction*

In vivo, most contractile cells adopt a polarized elongated morphology, characterized with strongly oriented SF (aligned along the principal direction of the cell) that drive the direction of contraction. The first example concentrates on such an elongated cell that deforms uniaxially and homogeneously in a constrained environment for which the details of the geometry and constraints are shown in Fig. 8. In this problem, cell-substrate adhesion is modeled as rigid connections between the cell and a set of linear elastic springs that characterize the stiffness of the underlying substrate. Because of its one-dimensional feature, this problem is used as a benchmark to assess how the proposed formulation captures cell contraction and quantify the influence of various model parameters.

The first analysis aims at evaluating the effect of the stiffness of the cell support (represented by the nondimensional parameter $K^\star = K/(\bar{T}\ell_0)$) on cell contraction. Fig. 9 shows the time evolution of cell deformation, contractile stress and fiber

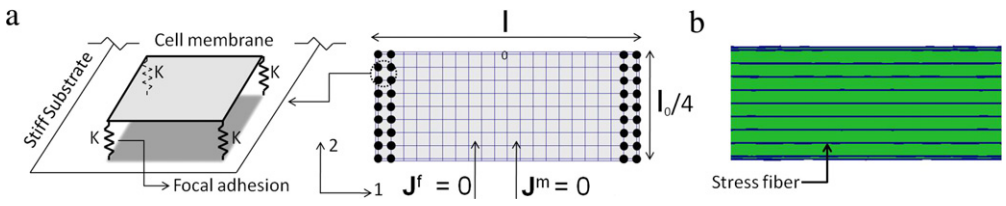

Fig. 8 – (a) The geometry of the cell and boundary conditions. The cell of length $l_0 = 40$ μm is free to contract in the vertical direction but is constrained in the horizontal direction by linear springs of stiffness K. (b) Generated SF at steady state.

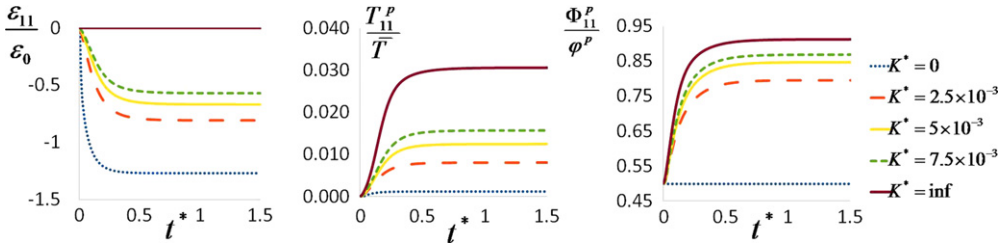

Fig. 9 – Time evolution of cell deformation, contractile stress and SF anisotropy for different values of support stiffness $K^\star$.

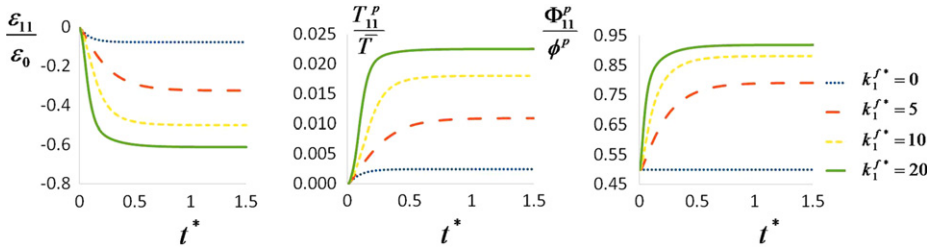

Fig. 10 – Time evolution of cell deformation, contractile stress and SF anisotropy for different values of mechano-sensitivity coefficient $k1^f$.

anisotropy for various values of $K^\star$ ranging from 0 to very large values. Generally these results show that from its original state (no contraction and no SF), a cell tends to develop a SF network and generate increasing contractile force in time, until it reaches a steady state. Furthermore, one can see that there is a clear relationship between cell contractility (represented by stress component T^p_{11}), SF anisotropy (Φ^p_{11}) and substrate stiffness $K^\star$. For large spring stiffness, the cell can only undergo very small strains (and strain rates), which results in a quasi-constant SF contraction as described by the length–tension and velocity–tension relationships. This large contraction, in turn, triggers the formation of additional fibers that contribute to a rise in contraction. Steady state is finally reached when the majority of G-actin monomers are consumed by the G-actin/SF reaction. On the contrary, a soft mechanical environment ($K^\star \to 0$) results in large contractile strains and a decrease in both fiber formation and contractile stress. Moreover, the distribution of SF (represented by Φ^p_{11}) varies from a totally isotropic network ($\Phi^p_{11}/\phi^p = 0.5$) to an extremely horizontally oriented network ($\Phi^p_{11}/\phi^p \to 1$) as spring stiffness increases. This clearly shows how SFs align in the directions of maximum stiffness.

The next analysis concentrates on assessing the role of mechano-sensitivity of SF formation (represented by the rate constant k^f_1 introduced in (36)) on cell contractility for a constant spring stiffness $K^\star = 0.01$ (Fig. 10). Since increasing k^f_1 promotes SF formation in the direction of maximum contraction, it is associated with a rise in fiber formation, contractile stress and deformation along the horizontal direction. We also note that when $k^{f\star}_1$ vanishes, SF formation is insensitive to contraction, which results in a totally isotropic fiber distribution ($\Phi^p_{11}/\phi^p = 0.5$) and a very low contraction (which arises from the rate of fiber formation k^f_0). This clearly shows that k^f_1 is a critical parameter in capturing the mechano-sensitivity of cell contraction.

To better understand the main trends exhibited by the model, the last analysis focuses on assessing the steady-state value of strain, contractile stress and fiber distribution variation with spring stiffness and rate constant $k^{f\star}_1$. The results displayed in Fig. 11 can be summarized as follows:

- Cell contraction increases with substrate stiffness in a nonlinear fashion until it reaches a maximum value. This value is determined by the initial quantity of actin monomers that can polymerize into SF.
- The intensity of cell contraction and deformation is determined by the mechano-dependent rate of fiber formation $k^{f\star}_1$ and the isometric stress $\bar{T}$ in each SF.

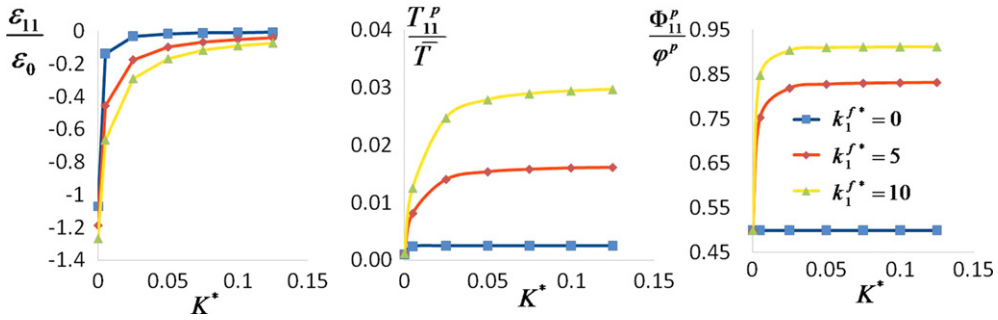

Fig. 11 – Effect of support stiffness on steady state cell deformation, contractile stress and SF anisotropy for different values of mechano-sensitivity coefficient $k1^{f\star}$.

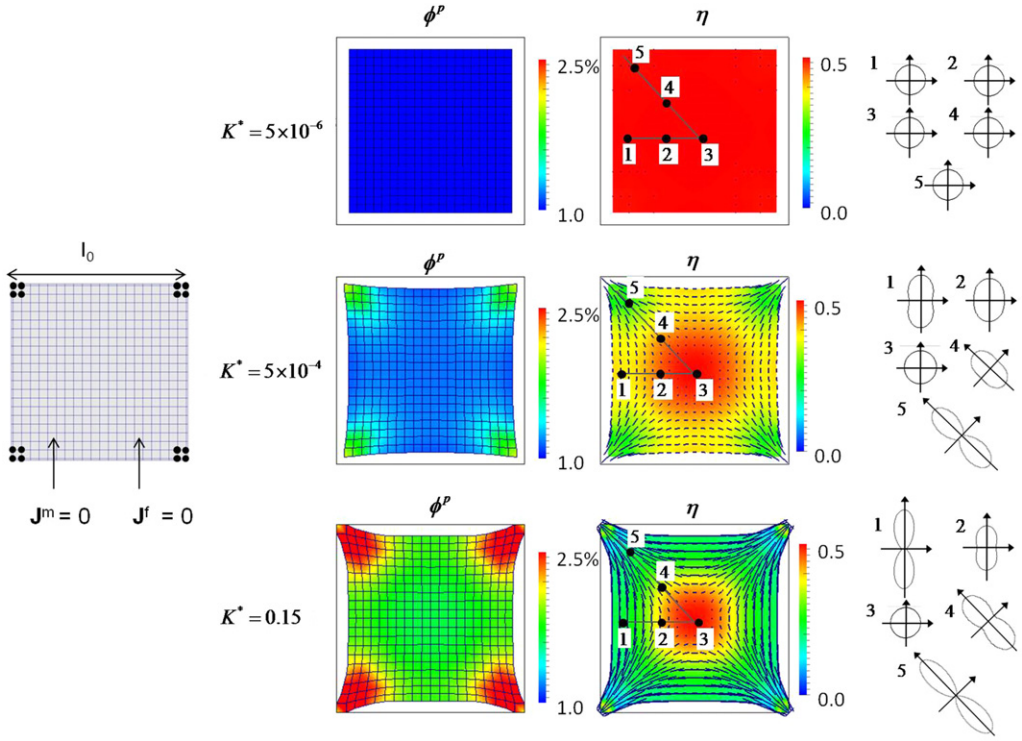

Fig. 12 – SF volume fraction φp and distribution at steady-state for three values of support stiffness (ranging from very low to very high). The principal direction of SFs are indicated by lines and the parameter η refers to the degree of anisotropy ($\eta = 0.5$ for an isotropic network and $\eta = 0$ for an unidirectional fiber direction). The polar fiber distribution $(\varphi^p(\theta))$ is also shown for 5 characteristic points in the cell.

- SF distribution becomes increasingly anisotropic with a rise in spring stiffness and mechano-dependent rate of fiber formation $k_1^{f\star}$. This is explained by the fact that new fibers are formed in the directions of maximum contractile stress, which in turn increases the contraction in this particular direction. This feedback mechanism is a key to understanding cell contraction.

5.3. *Contraction of a square cell attached at its corners*

The next example concerns the contraction of a square fibroblast that is constrained at its corners by elastic supports (Fig. 12) characterized by a non-dimensional stiffness $K^\star = K/(\bar{T}\ell_0)$. This situation has been previously studied both experimentally by Tan and coworkers Tan et al. (2003) as well as Bischofs et al. (2008) and theoretically by Deshpande et al. (2006, 2007). This example is particularly interesting since it involves heterogeneous cell deformation and the development of a spatially varying SF network. Further, due to the simple geometry and experimental reproducibility, this problem can be used as a benchmark to assess model prediction in terms of contraction, SF distribution and characteristic time-scales. The solution is obtained using a mixed-finite element procedure (Almeida and Spilker, 1997) for which nine node elements are used to describe solid velocity fields while four nodes are used to represent pressure

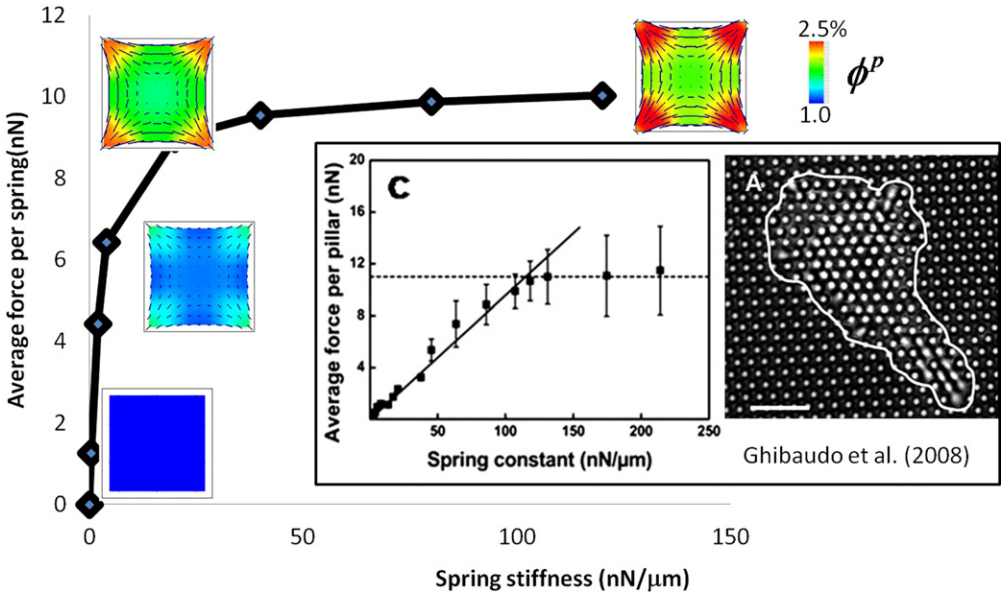

Fig. 13 – Steady-state contractile force F at focal adhesions as a function of support stiffness K as predicted with the proposed model. The steady-state morphology and corresponding SF distribution are are shown for characteristic values of K. For comparison, experimental results from Ghibaudo et al. (Ghibaudo et al., 2008) on the variation contractile forces in terms of pillar stiffness (spring constant) are also reported.

and actin monomer concentration. Large deformations are handled with an updated Lagrangian formulation, that consists of updating the reference configuration of the cell at each time step, therefore facilitating the treatment of the mapping between different material configurations (Belytschko et al., 2000). Finally, time integration is performed with an implicit Backward Euler integration scheme, coupled with a Newton procedure to obtain a solution at each time step. The presented results are obtained after discretizing the cell domain into nine-node elements as shown in Fig. 12. Element size was chosen to give satisfactory convergence while minimizing the computational cost. More details on this procedure are given in a companion paper (Farsad and Vernerey, in preparation).

Starting from out-of-equilibrium initial conditions ($\phi^p = 0$ at $t = 0$), the solution shows that cell contraction originally occurs at fast rates that tends to decay in time in order to reach a steady-state solution for which contraction is maximum. This choice initial condition (out-of equilibrium) is critical to observe cell contraction as it triggered the original SF formation, responsible for the beginning of the positive feedback loop described above. Indeed, no contraction is observed if the initial conditions satisfy both mechanical and chemical equilibrium. However, real cells are known to constantly be out-of-equilibrium, and a change in chemical equilibrium may be enough to start the positive feedback loop observed in the model. Our results suggest that support stiffness has a significant effect on SF formation and distribution. To illustrate this, Fig. 12 shows the steady-state cell deformation and the associated SF network for three characteristic support stiffness: $K^\star = 5 \cdot 10^{-6}$, $K^\star = 5 \cdot 10^{-4}$, and $K^\star = 0.15$. These results indicate that as $K^\star$ increases, the following observations can be made:

- SF concentration increases and their orientation is more and more pronounced along directions of maximum stiffness. Indeed, as substrate stiffness increases, boundary conditions on the cell range from an isotonic situation (the cell can deform under the load) to an isometric situation (the cell deformation is prescribed by its support). The velocity–tension relation indicates that the isometric situation results in the development of strong contractile stresses, which then promote the polymerization of SF (through the mechano-sensitive rate of formation). On the contrary, isotonic situation (especially at small stiffnesses) decreases contraction and consequently, SF formation.
- Cell morphology tends to become more "stellate" with increasing membrane curvature between attachments. In this context, we note that experimental observation of cell morphology exhibits a uniform curvature (Bischofs et al., 2008), a feature that is not predicted by the results shown in Fig. 12. This discrepancy can be attributed to the fact that surface elasticity of the cortical membrane has been neglected in the present model. However, we show in another study (Vernerey and Farsad, 2011) that including the effects of membrane elasticity result in uniform surface strains and curvature, consistent with experimental observations.
- Contractile forces applied to the external supports rise in a nonlinear fashion (Fig. 13) until they reach a maximum value (that can be shown to be determined by the initial amount of G-actin in the cell and the dissociation rate constant k_d). This result may be compared with experimental observations by Ghibaudo et al. (2008) of the dependency of cell contractility on support stiffness using micro-patterned substrates (micro-pillars). While a quantitative comparison cannot be established here due to differences in cell size and morphology, the results

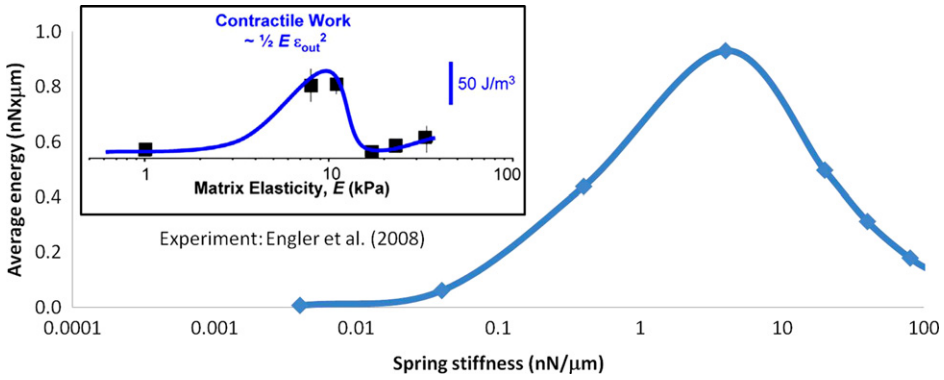

Fig. 14 – Mechanical work of the cell in terms of substrate stiffness: Qualitative comparison of model prediction and experiments on cardiomyocytes (Adam et al., 2008).

show that the model captures both the order of magnitude of contractile forces as well as the trends in substrate stiffness-cell contraction relationships.

An important consequence of the observed behavior is that the mechanical work performed by the cell is optimized for a specific range of substrate stiffness. To illustrate this, we computed the average work W done by the cell as:

$$W = 4F\delta \tag{63}$$

where F and δ are the average force and displacement of focal adhesion, respectively. The number 4 arises due to the fact that the square cell has four focal adhesions. Numerically computing W in terms of spring stiffness clearly shows that an optimum stiffness for our system is located around $1\ \text{nN}/\mu\text{m} \leq K \leq 10\ \text{nN}/\mu\text{m}$ as show in Fig. 14, a result that qualitatively correlates well with experimental studies on cardiac cell contractions (Adam et al., 2008). This behavior may be explained by the fact that at low substrate stiffness, very little force is generated by cells ($F \approx 0$) and thus no work is performed while at high stiffness, cell cannot generate substrate deformation ($\delta = 0$) which also implies a vanishing work. The intermediate substrate stiffness which optimizes both force and displacement is most of the time preferable for certain cell phenotypes. Understanding such processes is critical for the design optimized artificial gels for tissue engineering (Adam et al., 2008).

5.4. *Effect of cell morphology on cell SF structure*

Recent experiments on contractile cells (such as cardiomyocyte) have shown that a strong correlation exists between cell shape and structure (Bray et al., 2008; Parker et al., 2008), indicating that cell function, and in particular contractility, is strongly affected by geometrical factors. This section consists of assessing the prediction of the proposed model in that respect. For this, as a mean of comparison with experimental tests (Bray et al., 2008; Parker et al., 2008; Geisse et al., 2009; Bray et al., 2010), we consider three different cells (Fig. 15) each characterized by their own morphology (square, rectangular and triangular shapes) and focal adhesions distribution. In particular, we assume here that a cell adheres to a rigid substrate at specific locations (cell corners), which results in constraining the motion of material points on adhesion islands, represented by black dots in Fig. 15(a). Initial and boundary conditions are similar to those applied in the previous example.

As depicted in Fig. 15 the proposed model is able to capture the general SF organization observed in experiments for various cell morphology (Bray et al., 2008; Parker et al., 2008; Geisse et al., 2009; Bray et al., 2010). Both Fig. 15(b) and (c) show that SFs are mostly generated in directions that are restricted in terms of elongation, i.e. lines between the adhesion islands. As discussed in the previous section, this is explained by the fact that the rate of cytoskeleton's contraction along these directions is very small (close to zero) and thus promotes contractility and SF generation. Overall, these results indicate that interactions between SF formation and mechanics, as described by the proposed model, are sufficient to accurately reproduce key features of cell organization and force generation observed in the experiments.

6. Concluding remarks

To summarize, this paper presents a mixture framework that aims at describing the processes by which contractile cells are able to sense their mechanical environment (through stiffness) and react by adjusting the amount of contractile force they generate. By describing the cell's body as a mixture of four critical contractile elements, the proposed model is able to accurately capture the interplay between both mechanical and chemical mechanisms taking place in cells. The key features of the approach are:

- SF contraction is described by the velocity–tension and length–tension relationships arising from cross-bridge dynamics.
- SF formation arises from mass exchange with dispersed globular actin monomers and is assumed to depend on the tension in existing SF. This aspect is the main assumption of the model regarding the mechano-sensitivity of contraction. Cytosol and globular actin transport is described by conventional diffusion–convection type laws.
- Cell contraction is described in terms of both passive elasticity of the cytoskeleton and active contractile stress from a statistical distribution of SF.

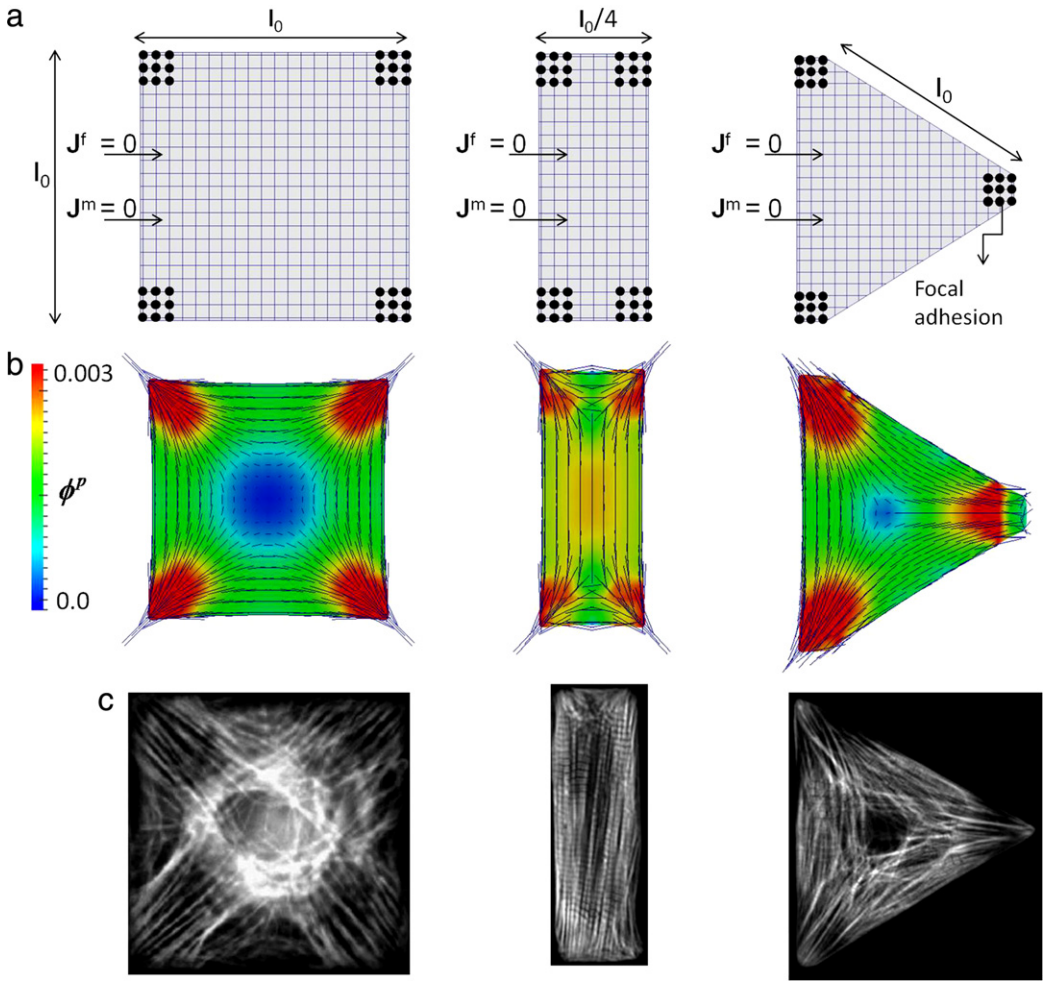

Fig. 15 – Effect of cell morphology on SF distribution. (a) Definition of focal adhesion complexes, boundary conditions and finite-element discretization ($0 = 40\ \mu m$). (b) Computed SF orientation and density for three different shapes and (c) comparison with experimental observations of fibril distribution in cardiomyocytes by Parker and co-workers Bray et al. (2008); Parker et al. (2008); Geisse et al. (2009); Bray et al. (2010).

The model exhibits a positive feedback mechanism resulting between the mechanical–chemical interplay between constituents. Contractile stress (that depends on strain-rate through the tension velocity relationship) promotes SF formation and SF formation results in increasing contraction. This loop eventually ends when the stock of available globular actin for SF formation is depleted. The solution to the model shows that this chemo-mechanical cross-talk could be responsible for the sensitivity of cell contraction on substrate stiffness. In other words, the proposed model may be used as a first step to characterize the interactions between a contractile cell and its environment, which is an important feature of the processes of tissue remodeling, would healing and morphogenesis. In addition, the present study has shown how multiscale principles (Vernerey et al., 2007) (homogenization) and multiphasic mixture concepts can be extended to investigate the active behavior of cells. This approach is very promising as various physical processes including chemistry, mechanics and transport and their interactions can be described in a consistent framework that satisfy basic conservation principles (balance of mass, momentum and energy).

Acknowledgment

FJV gratefully acknowledges the University of Colorado CRCW Seed Grant in support of this research.

REFERENCES

Almeida, E.S., Spilker, R.L., 1997. Mixed and penalty finite element models for the nonlinear behavior of biphasic soft tissues in finite deformational part 1—alternate formulations. Computer Methods in Biomechanics and Biomedical Engineering 1, 25–46.

Ateshian, G.A., Likhitpanichkul, M., Hung, C.T., 2006. A mixture theory analysis for passive transport in osmotic loading of cells. Journal of Biomechanics 39, 464–475.

Belytschko, T., Liu, W.K., Moran, B., 2000. Nonlinear Finite Elements for Continua and Structures. Wiley and Sons.

Biot, M.A., 1941. General theory of three-dimensional consolidation. Journal of Applied Physics 12, 155–164.

Biot, M.A., 1957. The elastic coefficients of the theory of consolidation. Journal of Astrophysics and Astronomy 24, 594–601.

Bischofs, I.B., Klein, F., Lehnert, D., Bastmeyer, M., Schwarz, U.S., 2008. Filamentous network mechanics and active contractility determine cell and tissue shape. Biophysical Journal 95, 3488–3496.

Bowen, R.M., 1980. Incompressible porous media models by the use of the theory of mixtures. International Journal of Engineering Science 18, 1129–1148.

Bray, M.P., Adams, W.J., Geisse, N.A., Feinberg, A.W., Sheehy, S.P., Parker, K.K., 2010. Nuclear morphology and deformation in engineered cardiac myocytes and tissues. Biomaterials 31, 5143–5150.

Bray, M., Sheehy, S.P., Parker, K.K., 2008. Sarcomere alignment is regulated by myocyte shape. Cell Motility and the Cytoskeleton 65, 641–651.

Carlson, F.D., Wilkie, D.R., 1974. Muscle Physiology. Prentice Hall.

Coussy, O., 2004. Poromechanics, third ed. John Wiley and Sons, Ltd..

Dallon, J.C., Ehrlich, H.P., 2008. A review of fibroblast-populated collagen lattices. Wound Repair and Regeneration 16, 472–479.

Deshpande, V.S., McMeeking, R.M., Evans, A.G., 2006. A bio-chemo-mechanical model for cell contractibility. PNAS 103 (38), 14015–14020.

Deshpande, V.S., McMeeking, R.M., Evans, A.G., 2007. A model for the contractility of the cytoskeleton including the effects of stress-fibre formation and dissociation. Proceedings of the Royal Society of London, Series A 463, 787–815.

Deshpande, V.S., Mrksich, M., McMeeking, R.M., Evans, A.G., 2008. A bio-mechanical model for coupling cell contractility with focal adhesion formation. Journal of the Mechanics and Physics of Solids 56, 1484–1510.

Engelke, R., Heinrich, D., Radler, J., 2010. Probing GFP-actin diffusion in living cells using fluorescence correlation spectroscopy. Physical Biology 7, 1–9.

Engler, Adam J., Carag-Krieger, Christine, Johnson, Colin P., Raab, Matthew, Tang, Hsin-Yao, Speicher, David W., Sanger, Joseph W., Sanger, Jean M., Discher, Dennis E., 2008. Embryonic cardiomyocytes beat best on a matrix with heart-like elasticity: scar-like rigidity inhibits beating. Journal of Cell Science 121, 3794–3802.

Farsad, M., Vernerey, F.J., 2010. A multiphysics computational formulation to describe cell-ecm mechanical interactions. International Journal for Numerical Methods in Engineering (in preparation).

Garikipati, K., Arruda, E.M., Grosh, K., Narayanan, H., Calve, S., 2004. A continuum treatment of growth in biological tissue: the coupling of mass transport and mechanics. Journal of the Mechanics and Physics of Solids 52, 1595–1625.

Gasser, T.C., Ogden, R.W., Holzapfel, G.A., 2006. Hyperleastic modelling of arterial layers with distributed collagen fibre orientations. Journal of the Royal Society Interface 3, 15–35.

Geisse, N.A., Sheehy, S.P., Parker, K.K., 2009. Control of myocyte remodeling in vitro with engineered substrates. In Vitro Cellular & Developmental Biology—Animal 45, 343–350.

Ghibaudo, Marion, Saez, Alexandre, Trichet, Léa, Xayaphoummine, Alain, Browaeys, Julien, Silberzan, Pascal, Buguinb, Axel, Ladoux, Benoît, 2008. Traction forces and rigidity sensing regulate cell functions. Soft Materials 4, 1836–1843.

Guilak, F., Haider, M.A., Setton, L.A., Laursen, T.A., Baaijens, F.P.T., 2006. Multiphasic models of cell mechanics. In: Cytoskeletal Mechanics: Models and Measurements. Cambridge University Press, pp. 84–102.

Guilak, F., Mow, V.C., 2000. The mechanical environment of the chondrocyte: a biphasic finite element model of cell-matrix interactions in articular cartilage. Journal of Biomechanics 33, 1663–1673.

Gu, W.Y., Lai, W.M., Mow, V.C., 1999. Transport of multi-electrolytes in charged hydrated biological soft tissues. Transport in Porous Media 34, 143–157.

Guo, W.H., Frey, M.T., Burnham, N.A., Wang, Y.L., 2006. Substrate rigidity regulates the formation and maintenance of tissues. Biophysical Journal 90, 2213–2220.

Hill, A.V., 1938. The heat of shortening and the dynamic constant of muscles. Proceedings of the Royal Society of London, Series B 126, 136–195.

Humphrey, J.D., Rajagopal, K.R., 2002. A constrained mixture model for growth and remodeling of soft tissues. Mathematical Models and Methods in Applied Sciences 12, 407–430.

Kumar, Sanjay, Maxwell, Iva Z., Heisterkamp, Alexander, Polte, Thomas R., Lele, Tanmay P., Salanga, Matthew, Mazur, Eric, Ingber, Donald E., 2006. Viscoelastic retraction of single living stress fibers and its impact on cell shape, cytoskeletal organization, and extracellular matrix mechanics. Biophysical Journal 90 (10), 3762–3773.

Lambert, A., Nusgens, B.V., Lapiere, M., 1998. Mechano-sensing and mechano-reaction of soft connective tissue cells. Advances in Space Research 21 (8–9), 1081–1091.

Levental, I., Georges, P.C., Janmey, P.A., 2006. Soft biological materials and their impact on cell function. Soft Matter 2, 1–9.

Menzel, A., Harrysson, M., Ristinmaa, M., 2008. Towards an orientation-distribution-based multi-scale approach for remodelling biological tissues. Computer Methods in Biomechanics and Biomedical Engineering 11 (5).

Mohrdieck, C., Wanner, A., Wouter, R., Roth, A., Sackmann, E., Spatz, J., Arzt, E., 2005. A theoretical description of elastic pillar substrates in biophysical experiments. ChemPhysChem 6, 1492–1498.

Na, S., Meininger, G.A., Humphrey, J.D., 2007. A theoretical model for F-actin remodeling in vascular smooth muscle cells subjected to cyclic stretch. Journal of Theoretical Biology 246, 87–99.

Nelson, C.M., Jean, R.P., Tan, J.L., Liu, W.F., Snladeckl, N.J., Spector, A.A., Chen, C.S., 2005. Emergent patterns of growth controlled by multicellular form and mechanics. PNAS 102 (33), 11594–11599.

Parker, Kevin Kit, Tan, John, Chen, Christopher S., Tung, Leslie, 2008. Myofibrillar architecture in engineered cardiac myocytes. Journal of the American Heart Association 103, 340–342.

Rajagopal, K.R., Tao, L., 1995. Mechanics of mixture. Series on Advances in Mathematics for Applied Sciences 35.

Rajagopal, K.R., Wineman, A.S., 1990. Development in the mechanics of interactions between a fluid and a highly elastic solid. In: Recent Development in Structured Continua, vol. II. Longman Scientific and Technical, New York, pp. 249–292.

Rubinstein, B., Jacobson, K., Mogilner, A., 2005. Multiscale two-dimensional modeling of a motile simple-shaped cell. Multiscale Modeling & Simulation 3 (2), 413–439.

Solon, J., Levental, I., Sengupta, K., Georges, P.C., Janmey, P.A., 2007. Fibroblast adaptation and stiffness matching to soft elastic substrates. Biophysical Journal 93, 4453–4461.

Sun, D.N., Gu, W.Y., Guo, X.E., Lai, W.M., Mow, V.C., 1999. A mixed finite element formulation of triphasic mechano-electromechanical theory for charged, hydrated biological soft tissues. International Journal for Numerical Methods in Engineering 45, 1375–1402.

Tamariz, E., Grinnell, F., 2002. Modulation of fibroblast morphology and adhesion during collagen matrix remodeling. Molecular Biology of the Cell 13, 3915–3929.

Tan, J.L., Tien, J., Pirone, D.M., Gray, D.S., Bhadriraju, K., Chen, C.S., 2003. Cells lying on a bed of microneedles: an approach to isolate mechanical force. Proceedings of the National Academy of Sciences of the United States of America 100, 1484–1489.

Terzaghi, K., 1943. Theoretical Soil Mechanics. Wiley, New York, Chapman and Hall, London.

Truesdell, C., Noll, W., 1965. Non-Linear Field Theories of Mechanics. In: Handbuch des Physik, Springer, Berlin, pp. 537–541.

Tsuda, Y., Yasutake, H., Ishijima, A., Yanagida, T., 1996. Torsional rigidity of single actin filaments and actin–actin bond breaking force under torsion measured directly by in vitro micromanipulation. PNAS 93, 12937–12942.

Vernerey, F.J., 2010. On the application of multiphasic theories to the problem of cell-substrate mechanical interactions. Advances in Cell Mechanics.

Vernerey, F.J., Farsad, M., 2011. An Eulerian/xfem formulation for the large deformation of cortical cell membrane. Computer Methods in Biomechanics and Biomedical Engineering 14 (5), 433–445.

Vernerey, F.J., Greenwald, E., Bryant, S., 2011. Triphasic mixture model of cell-mediated enzymatic degradation of hydrogels. Computer Methods in Biomechanics and Biomedical Engineering (in press).

Vernerey, F.J., Liu, W.K., Moran, B., 2007. Multi-scale micromorphic theory for hierarchical materials. Journal of the Mechanics and Physics of Solids 55, 2603–2651.

Wang, H.B., Dembo, M., Wang, Y.L., 2000. Substrate flexibility regulates growth and apoptosis of normal but not transformed cells. American Journal of Physiology—Cell Physiology 279, C1345–C1350.

Weiss, P., Garber, B., 1952. Shape and movement of mesenchyme cells as functions of the physical structure of the medium. contribution to a quantitative morphology. Zoology 38, 264–280.

White, Glenn E., Fujiwara, Keigi, 1986. Expression and intracellular distribution of stress fibers in aortic endothelium. The Journal of Cell Biology 103, 63–70.